To appear in *Philosophical Magazine Letters* Vol. 00, No. 00, Month 20XX, 1–9

Concurrent atomistic-continuum simulations of uniaxial compression of gold nano/submicropillars

Shuozhi Xu^{a*}, Marat I. Latypov^{b,c} and Yanqing Su^c

^a California NanoSystems Institute, University of California, Santa Barbara, Santa Barbara, CA 93106-6105, USA; ^b Materials Department, University of California, Santa Barbara, Santa Barbara, CA 93106-5050, USA; ^c Department of Mechanical Engineering, University of California, Santa Barbara, Santa Barbara, CA 93106-5070, USA

(July 31, 2018)

In this work, uniaxial compression of nano/submicropillars in Au with the initial diameter D between 26.05 and 158.53 nm was modeled by concurrent atomistic-continuum simulations. Two models with distinct surface facets were employed to explore the surface facets-dependent extrinsic size effects on the plastic deformation of pillars. It is found that (i) the yielding in pillars with smooth surface was controlled by dislocation nucleation from the two ends of the pillars, and (ii) in pillars with faceted surfaces, dislocations were initiated from the sharp edges on the surface. As a result of the differences in the plastic deformation mechanism between the two models, the yield stress decreases exponentially and increases nearly linearly with respect to an increasing D in pillars with smooth and faceted surfaces, respectively.

Keywords: Concurrent atomistic-continuum method; uniaxial compression; nano/submicropillar

1. Introduction

Extrinsic size effects on mechanical properties of materials due to dimensional constraints are ubiquitous in a wide range of engineering applications [1]. For example, the yield/flow of micro and nanopillars that are important in microelectronic engineering are known to depend on the diameter D, a topic that has been pursued by researchers via both experiments [2–5] and modeling [6, 7]. In nano and submicronsized pillars, i.e., $D \le 100$ nm and 100 nm $< D \le 1$ μ m, respectively, the specific plastic deformation mechanism during uniaxial loading — either dislocation slip, twinning, or phase transformation — may vary as D changes. In particular, when dislocation slip controls the plastic deformation, experiments in face-centered cubic (FCC) Au revealed that pillars with smaller D generally exhibit higher yield and flow strengths, a phenomenon usually attributed to either the dislocation starvation [2] or the dislocation source-limited behavior [8]. Experiments also found that in FCC metallic nanopillars, atomic-scale {111} facets are formed on the surface [9], which is characteristic of the dislocation nucleation events [10]. Because it is difficult to obtain in situ atomic trajectory inside the materials in experiments, numerical simulations via atomistic methods [11, 12] and discrete dislocation dynamics

^{*}Corresponding author. Email: shuozhixu@ucsb.edu

(DDD) [13, 14] have been conducted to shed light on the underlying mechanisms of the extrinsic size effects in deformed pillars. For example, previous atomistic simulations in Au found that atomic-scale {111} surface facets reduce the strength of $\langle 111 \rangle$ -oriented single crystalline nanopillars [15] while introducing large {111} surface facets increases the strength of $\langle 111 \rangle$ -oriented nanotwinned nanopillars [11, 12]. To our best knowledge, it remains unexplored how large surface facets affect the plastic deformation of single crystalline FCC nano/submicropillars, and particularly those of $\langle 100 \rangle$ -oriented type. We remark that the axial crystallographic orientation may greatly influence the operative deformation mechanisms of the pillars [16].

With these modeling techniques, however, it is challenging to consider submicropillars due to the trade-off between significant computational demands of atomistic simulations and the uncertainty inherent in continuum-based DDD. Indeed, to the best of our knowledge, the largest atomistic pillar model in the literature contained about 45 million atoms [6, 7], with the corresponding D = 70 nm, representing a nanopillar. On the other hand, while DDD [17] has become a popular choice to address the dislocation dynamics in deformation of submicro/micropillars, its predictive capability is strongly affected by the empirical parameters and rules introduced for short-range dislocation interactions. In light of this trade-off, in this Letter, we employ a multiscale materials modeling technique named the concurrent atomistic-continuum (CAC) method [18–20] to combine atomic-level accuracy with mesoscale efficiency. As a partitioned-domain method, the CAC simulation domain usually consists of an atomistic domain and a coarse-grained domain. Compared with most other multiscale approaches, CAC has the advantage of enabling the representation of certain lattice defects (e.g., dislocations and intrinsic stacking faults) in the coarse-grained domain without the need of mesh refinement [21]. Moreover, the same interatomic potential is introduced into both atomistic and coarse-grained domains as the only constitutive rule for dislocation dynamics.

In recent years, the CAC approach has been employed for coarse-grained modeling of a series of thermo and mechanical problems at the nano/submicron length scales in a wide range of materials [22]. In pure metals, CAC has been adopted to simulate brittle-to-ductile transition in dynamic fracture [21], surface indentation [20], dislocation nucleation from notches [23], quasistatic [20], subsonic [21], and transonic [24] dislocation migration in a lattice, screw dislocation cross-slip [25], dislocation/void interactions [26], dislocation/stacking fault interactions [27], dislocation/grain boundary interactions [28, 29], dislocations bowing out from obstacles [30], and dislocation multiplication from Frank-Read sources [31]. The success of these calculations suggests the viability of the CAC method for tackling complex dislocation-mediated metal plasticity problems [32]. In this work, large scale CAC simulations will be carried out to investigate compressive loading of nano/submicron-sized pillars in Au with D up to 158.53 nm.

2. Materials and Methods

Two CAC models, illustrated in Figure 1, were adopted to represent pillars; all boundaries of the simulation cell were assumed traction-free. In the coarse-grained domain, discontinuous 3D rhombohedral finite elements with all surfaces laying on the slip planes of the lattice, which are {111} planes in FCC systems, to accommodate dislocation slip between elements, among which no interelement compatibility was required. In Model-A, only finite elements, each of which contains 2197 atoms,

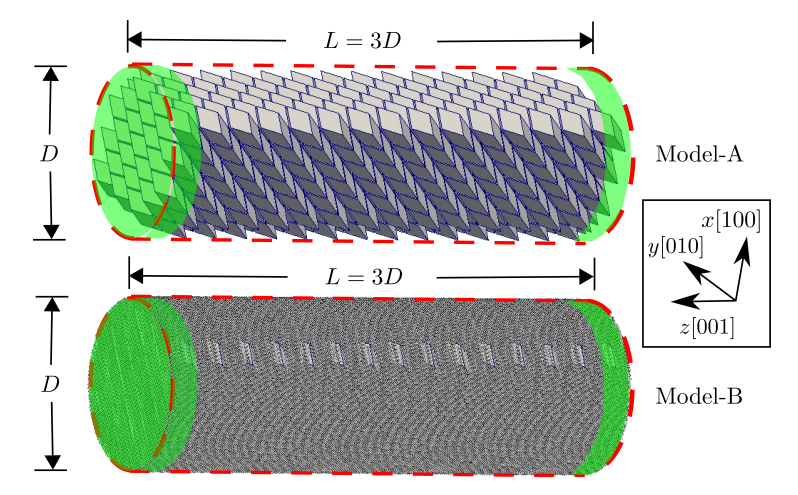


Figure 1. Two CAC models of nanopillars in FCC Au with D=26.05 nm. In Model-A, the simulation cell consisted of only finite elements, and so the surface was faceted; in Model-B, an atomistic domain was introduced to 'fill in' the interstices between the boundary of a cylinder and the element boundaries. In both models, the atoms/nodes within the green regions were not allowed to move along the z direction after each incremental compressive strain was affinely applied to the whole pillar.

were employed. As a result of the element shape, the pillars naturally had $\{111\}$ faceted surfaces. In Model-B, discrete atoms were introduced to 'fill in' the interstices between the element boundaries in Model-A and the boundary of a cylinder. For both models, the pillar diameter D varied from 26.05 to 158.53 nm, while a fixed length-to-diameter ratio of 3 was maintained. An embedded-atom method (EAM) potential [33] was employed to calculate the interatomic forces and energies, with a lattice constant $a_0 = 4.0701$ Å. We remark that the interatomic potential plays a crucial role in atomistic simulations [34–36] and the selected EAM potential has been adopted to investigate uniaxial deformation of Au nanopillars [11, 12]. Consequently, the simulation cell, with all three axes along $\langle 100 \rangle$ directions, contained up to 559.12 million atoms in an equivalent fully-resolved atomistic model.

After the systems were energy minimized using a conjugate gradient algorithm [20], dynamic CAC simulations were run with a constant compressive strain rate of 10^9 s⁻¹ imposed on each pillar along the axial z direction at 10 K. Specifically, within each time step (5 fs), the whole pillar was first affinely compressed, then atoms/nodes near both ends of each pillar (the green regions in Figure 1) were not allowed to move along the z direction during the same velocity Verlet iteration. In other words, all atoms/nodes were allowed to freely move within the x-y plane all the time. The engineering stress was calculated by dividing the total virial of the system by the real-time simulation cell volume. All simulations were conducted using PyCAC [37, 38]; for post-processing purpose, the atomic positions inside the finite elements were interpolated from the nodes in the coarse-grained domain and visualized by OVITO [39]. Note that the PyCAC code has been extensively benchmarked against atomistic simulations in terms of static dislocation properties and dislocation dynamics including, but not limited to, the generalized stacking fault energy surface, dislocation core structure/energy/stress fields, Peierls stress, and dislocation array migration across the atomistic/coarse-grained domain interface [20, 31]. Here, for the pillar models with D = 26.05 nm, equivalent molecular dynamics (MD) simulations have been carried out using LAMMPS [40]. Note that while MD and CAC simulations predict somewhat different stress-strain curves, the yield stress and dislocation dynamics are well represented in CAC simulations.

3. Results and Discussion

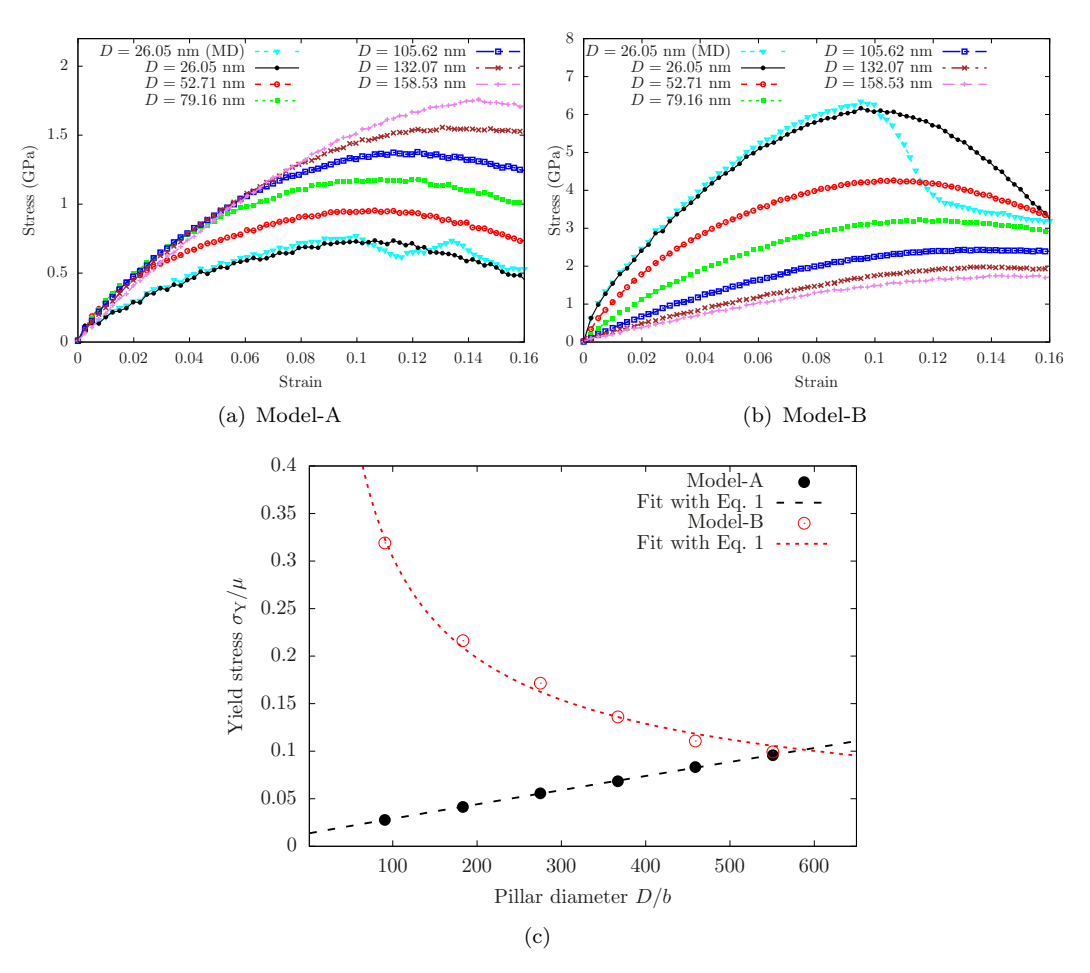


Figure 2. Stress–strain curves of (a) Model-A and (b) Model-B. (c) Yield stresses σ_{Y} , normalized by the isotropic shear modulus $\mu = 27$ GPa and taken at the strain subject to which dislocations started to nucleate from the traction-free surfaces, are plotted with respect to the initial pillar diameter D which is normalized by the magnitude of the Burgers vector of the full dislocation $b = a_0/\sqrt{2} = 0.288$ nm.

The stress-strain responses for the two models are plotted in Figure 2(a-b). The yield stresses, $\sigma_{\rm Y}$, taken at the strain subject to which dislocations started to nucleate from the traction-free surfaces, are summarized in Figure 2(c) with respect to the initial pillar diameter D. It is shown that (i) for the same D, Model-A had a lower $\sigma_{\rm Y}$ than Model-B and (ii) $\sigma_{\rm Y}$ increased and decreased with an increasing D for Model-A and Model-B, respectively. A power law relation, which was confirmed by numerous experiments to be universal between the yield/flow stress and sample size in small-sized metallic systems regardless of fabrication technique [1], was used to fit the CAC-predicted σ_{Y} -D data set with three parameters σ_{0} , k, and n, i.e.,

$$\sigma_{\mathcal{Y}}(D) = \sigma_0 + kD^n \tag{1}$$

which yielded n = 0.98 and -0.62 for Model-A and Model-B, respectively. In other words, $\sigma_{\rm Y}$ increased nearly linearly with D for Model-A while decreased exponentially with D for Model-B, as a result of their different surface facets. In previous experiments which applied a compressive loading on pillars with relatively smooth surfaces, i.e., more alike Model-B than Model-A, the power law slope n=-0.97 for submicropillars [41] and -0.66 for micropillars [42] in Au, the latter of which was close to the CAC-predicted value for Model-B. This faceted surface-induced change in the extrinsic size effect in nano/submicropillars was the key finding of this work. Note that the two fit curves in Figure 2(c) were extrapolated to intersect at D=168.67 nm, for which the surface facets magnitude for Model-A, 0.02D, was negligible.

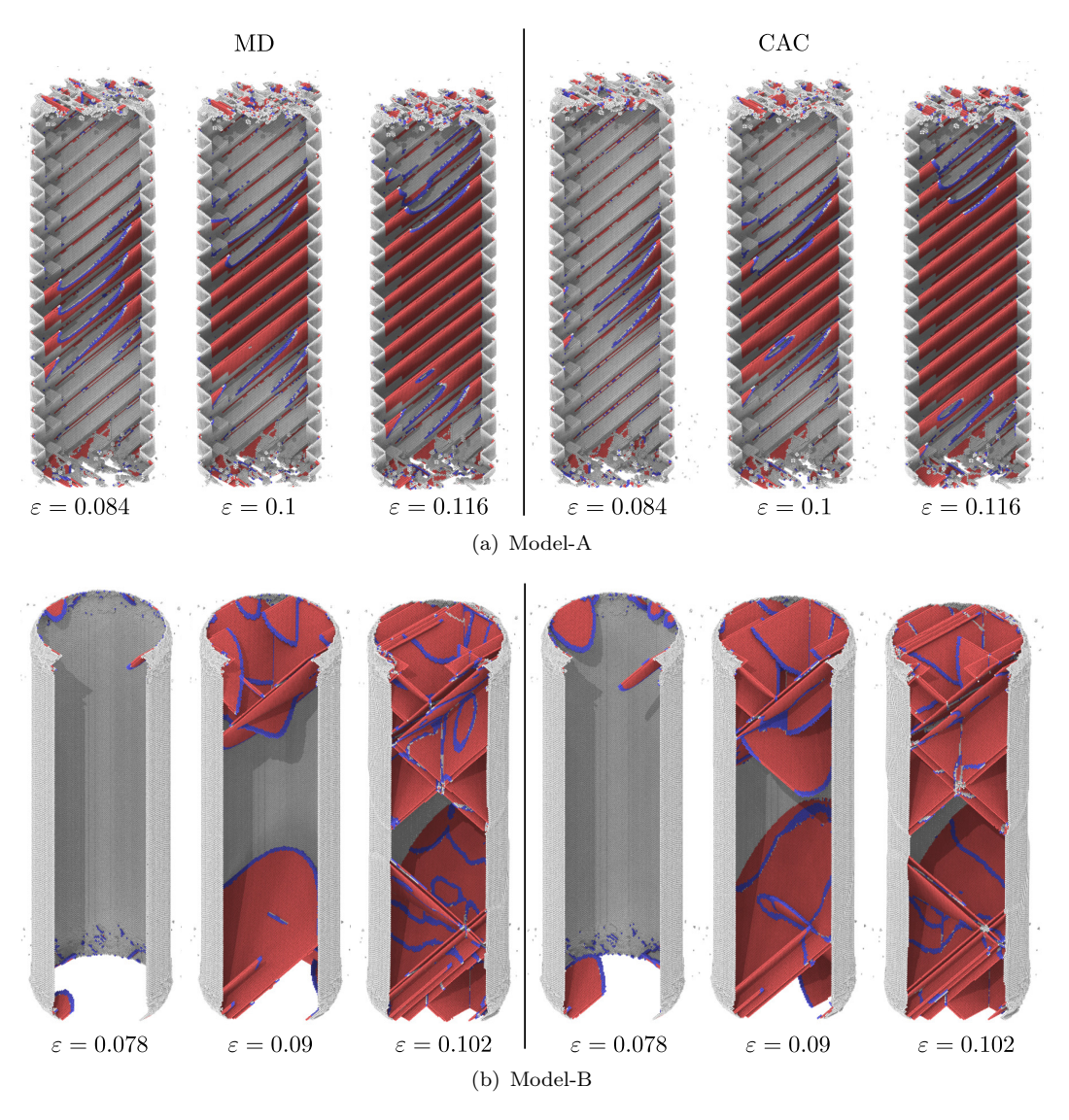


Figure 3. MD- and CAC-predicted atomistic structures of the nanopillar with D=26.05 nm for (a) Model-A and (b) Model-B. Note that for CAC simulation results, in the coarse-grained domain, atoms within elements are linearly interpolated from the nodal positions. Atoms are colored by a-CNA [43]: red and blue are for atoms in hexagonal close-packed and body-centered cubic lattices, respectively, the atoms on the traction-free surfaces are in white, and all FCC atoms are deleted.

Atomistic structures in the vicinity of the yield point in both models were analyzed by adaptive common neighbor analysis (a-CNA) [43], as shown in Figure 3. In Model-A, the faceted surface formed a 'spring-like' structure, which withstood some compressive strain before multiple dislocations on parallel {111} planes were nucleated from the sharp edges on the faceted surface. Since pillars with a larger

D contained a larger number of surface facets, they were able to endure a larger amount of elastic compression before yielding occurred; thus the yield stress increased with D. In Model-B, the yielding corresponded to the nucleation of dislocations on different $\{111\}$ planes from the intersections between the cylinder surface and top/bottom caps. With an increasing D, the perimeter of the caps, and hence the number of dislocation sources, increased. This change in the dislocation source number, along with the fact that larger pillars have a smaller Young's modulus due to the lower residual stress on the surface [44], resulted in a lower yield stress for pillars with a larger D. Between the two models, the differences in their underlying plastic deformation mechanisms may be the reason why their pillar size effects on the yield stress differ.

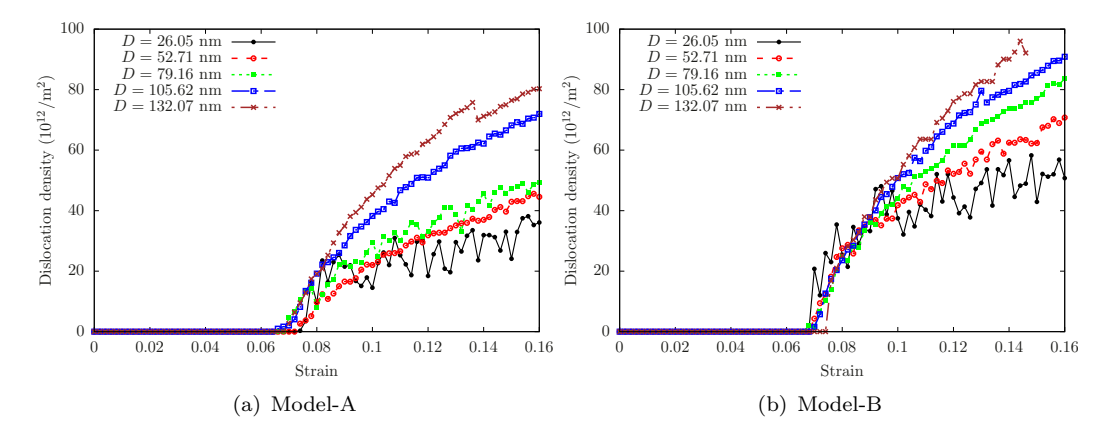


Figure 4. Evolution of dislocation density, calculated by a dislocation extraction algorithm [45], with strain for different initial pillar parameter D of (a) Model-A and (b) Model-B.

To calculate the dislocation density, we applied a dislocation extraction algorithm [45] to the atomistic structures, as shown in Figure 4. It is found that, at the same strain, (i) for the same D, the dislocation density in Model-A was lower than that in Model-B, corresponding to the rapid dislocation avalanches shown in Figure 3(b) and (ii) for both models, pillars with a larger D generally had a higher dislocation density; no dislocation starvation was observed.

4. Conclusion

In this work, large scale CAC simulations were conducted to explore the extrinsic size effects on the compressive plastic deformation of nano/submicropillars in Au. Two models with different types of surface were considered: in Model-A, only rhombohedral finite elements were employed and so the surfaces were faceted on {111} planes; in Model-B, the faceted surface in Model-A was 'smoothened' by filling in atoms. For both models, the pillar diameter D varied from 26.05 to 158.53 nm. It is found that (i) for the same D, Model-A has a lower yield stress, $\sigma_{\rm Y}$, than Model-B and (ii) with respect to an increasing D, $\sigma_{\rm Y}$ increases almost linearly in Model-A while decreases exponentially in Model-B. Analyzing the atomistic structures attributed the above findings to the different plastic deformation in the two models: in Model-A, the yielding was controlled by dislocation nucleation from the faceted surfaces which formed a 'spring-like' structure and so a larger pillar was able to withstand larger amount of elastic compressive strain prior to yielding; in Model-B,

pillar au cac

the initial dislocations were nucleated from the intersections between the cylinder surface and the top/bottom caps, hence a larger pillar contained more dislocation source which, along with its smaller Young's modulus, led to a lower yield stress. Our work highlights the significance of considering the surface facets in investigating the extrinsic size effects on the yield/flow of metallic nano/submicropillars. Additional extrinsic size effects such as the wall thickness in the nano/submicrotubes [46] will be explored in the future.

Disclosure

The authors declare no conflict of interest.

Acknowledgement

The authors thank Mr. Rui Che for helpful discussions. The work of SX was supported in part by the Elings Prize Fellowship in Science offered by the California NanoSystems Institute (CNSI) on the UC Santa Barbara campus. SX and MIL acknowledge support from the Center for Scientific Computing from the CNSI, MRL: an NSF MRSEC (DMR-1121053). This work used the Extreme Science and Engineering Discovery Environment (XSEDE), which is supported by National Science Foundation grant number ACI-1053575.

References

- [1] J.R. Greer and J.T.M. De Hosson, Prog. Mater. Sci. 56 (2011) p. 654, Available at http://www.sciencedirect.com/science/article/pii/S0079642511000065.
- [2] J.R. Greer and W.D. Nix, Phys. Rev. B 73 (2006) p. 245410, Available at http: //link.aps.org/doi/10.1103/PhysRevB.73.245410.
- [3] J.R. Greer, C.R. Weinberger and W. Cai, Mater. Sci. Eng. A 493 (2008) p. 21, Available at http://www.sciencedirect.com/science/article/pii/S0921509307019302.
- [4] J.R. Greer, J.Y. Kim and M.J. Burek, JOM 61 (2009) p. 19, Available at http:// link.springer.com/article/10.1007/s11837-009-0174-8.
- [5] J.Y. Kim and J.R. Greer, Acta Mater. 57 (2009) p. 5245, Available at http://www. sciencedirect.com/science/article/pii/S1359645409004510.
- [6] S. Xu, J.K. Startt, T.G. Payne, C.S. Deo and D.L. McDowell, J. Appl. Phys. 121 (2017) p. 175101, Available at http://aip.scitation.org/doi/10.1063/1.4982754.
- [7] S. Xu, Y. Su, D. Chen and L. Li, Appl. Phys. A 123 (2017) p. 788, Available at https://link.springer.com/article/10.1007/s00339-017-1414-3.
- [8] C.A. Volkert and E.T. Lilleodden, Philos. Mag. 86 (2006) p. 5567, Available at http: //dx.doi.org/10.1080/14786430600567739.
- [9] M. Tian, J. Wang, J. Kurtz, T.E. Mallouk and M.H.W. Chan, Nano Lett. 3 (2003) p. 919, Available at https://doi.org/10.1021/n1034217d.
- [10] B. Hyde, H.D. Espinosa and D. Farkas, JOM 57 (2005) p. 62, Available at https: //link.springer.com/article/10.1007/s11837-005-0118-x.
- [11] C. Deng and F. Sansoz, ACS Nano 3 (2009) p. 3001, Available at http://dx.doi. org/10.1021/nn900668p.
- [12] C. Deng and F. Sansoz, Phys. Rev. B 81 (2010) p. 155430, Available at https://link. aps.org/doi/10.1103/PhysRevB.81.155430.

- [13] S. Papanikolaou, H. Song and E. Van der Giessen, J. Mech. Phys. Solids 102 (2017) p. 17, Available at http://www.sciencedirect.com/science/article/pii/ S0022509616304112.
- [14] Y. Cui, G. Po and N. Ghoniem, Phys. Rev. B 95 (2017) p. 064103, Available at https://link.aps.org/doi/10.1103/PhysRevB.95.064103.
- [15] E. Rabkin and D.J. Srolovitz, Nano Lett. 7 (2007) p. 101, Available at http://dx. doi.org/10.1021/nl0622350.
- [16] C.R. Weinberger and W. Cai, J. Mater. Chem. 22 (2012) p. 3277, Available at https://pubs.rsc.org/en/content/articlelanding/2012/jm/c2jm13682a.
- [17] V. Bulatov and W. Cai, Computer simulations of dislocations, Oxford University Press, Oxford; New York, 2006 Dec.
- [18] Y. Chen, J. Chem. Phys. 130 (2009) p. 134706, Available at http://jcp.aip.org/resource/1/jcpsa6/v130/i13/p134706_s1.
- [19] L. Xiong, G. Tucker, D.L. McDowell and Y. Chen, J. Mech. Phys. Solids 59 (2011) p. 160, Available at http://www.sciencedirect.com/science/article/pii/ S0022509610002395.
- [20] S. Xu, R. Che, L. Xiong, Y. Chen and D.L. McDowell, Int. J. Plast. 72 (2015) p. 91, Available at http://www.sciencedirect.com/science/article/pii/ S0749641915000777.
- [21] S. Xu, L. Xiong, Q. Deng and D.L. McDowell, Int. J. Solids Struct. 90 (2016) p. 144, Available at http://www.sciencedirect.com/science/article/pii/ S0020768316300154.
- [22] S. Xu, J. Rigelesaiyin, L. Xiong, Y. Chen and D.L. McDowell, Generalized continua concepts in coarse-graining atomistic simulations, in Generalized Models and Non-classical Approaches in Complex Materials 2, Advanced Structured Materials, Springer, Cham, 2018, p. 237, Available at https://link.springer.com/chapter/10.1007/978-3-319-77504-3_12.
- [23] H. Chen, S. Xu, W. Li, R. Ji, T. Phan and L. Xiong, Comput. Mater. Sci. 144 (2018) p. 1, Available at https://www.sciencedirect.com/science/article/pii/ S0927025617306845.
- [24] L. Xiong, J. Rigelesaiyin, X. Chen, S. Xu, D.L. McDowell and Y. Chen, Acta Mater. 104 (2016) p. 143, Available at http://www.sciencedirect.com/science/article/pii/S1359645415300884.
- [25] S. Xu, L. Xiong, Y. Chen and D.L. McDowell, Acta Mater. 122 (2017) p. 412, Available at http://www.sciencedirect.com/science/article/pii/S1359645416307601.
- [26] L. Xiong, S. Xu, D.L. McDowell and Y. Chen, Int. J. Plast. 65 (2015) p. 33, Available at http://www.sciencedirect.com/science/article/pii/S0749641914001508.
- [27] S. Xu, L. Xiong, Y. Chen and D.L. McDowell, Crystals 7 (2017) p. 120, Available at http://www.mdpi.com/2073-4352/7/5/120.
- [28] S. Xu, L. Xiong, Y. Chen and D.L. McDowell, npj Comput. Mater. 2 (2016) p. 15016, Available at http://www.nature.com/articles/npjcompumats201516.
- [29] S. Xu, L. Xiong, Y. Chen and D.L. McDowell, JOM 69 (2017) p. 814, Available at https://link.springer.com/article/10.1007/s11837-017-2302-1.
- [30] S. Xu, L. Xiong, Y. Chen and D.L. McDowell, Scr. Mater. 123 (2016) p. 135, Available at http://www.sciencedirect.com/science/article/pii/S135964621630272X.
- [31] S. Xu, L. Xiong, Y. Chen and D.L. McDowell, J. Mech. Phys. Solids 96 (2016) p. 460, Available at http://www.sciencedirect.com/science/article/pii/S0022509616301016.
- [32] S. Xu and X. Chen, Int. Mater. Rev. 0 (2018) p. 1, Available at https://doi.org/ 10.1080/09506608.2018.1486358.
- [33] G. Grochola, S.P. Russo and I.K. Snook, J. Chem. Phys. 123 (2005) p. 204719, Available at http://aip.scitation.org/doi/10.1063/1.2124667.
- [34] S.Z. Chavoshi, S. Xu and S. Goel, Proc. R. Soc. A 473 (2017) p. 20170084, Available at http://rspa.royalsocietypublishing.org/content/473/2202/20170084.

- [35] S. Xu, S.Z. Chavoshi and Y. Su, Phys. Status Solidi RRL 12 (2018) p. 1700399, Available at https://onlinelibrary.wiley.com/doi/abs/10.1002/pssr.201700399.
- [36] S. Xu and Y. Su, Phys. Lett. A 382 (2018) p. 1185, Available at http://www. sciencedirect.com/science/article/pii/S0375960118302287.
- [37] S. Xu, T.G. Payne, H. Chen, Y. Liu, L. Xiong, Y. Chen and D.L. Mc-Dowell, J. Mater. Res. 33 (2018) p. 857, Available at https://www. cambridge.org/core/journals/journal-of-materials-research/article/ pycac-the-concurrent-atomisticcontinuum-simulation-environment/ E664F7A8C0AD8DD1673BE2BDE592D0AA.
- [38] S. Xu, PyCAC User's Manual, http://www.pycac.org/(2017), accessed: 07/31/2018.
- [39] A. Stukowski, Modelling Simul. Mater. Sci. Eng. 18 (2010) p. 015012, Available at http://iopscience.iop.org/0965-0393/18/1/015012.
- [40] S. Plimpton, J. Comput. Phys. 117 (1995) p. 1, Available at http://www. sciencedirect.com/science/article/pii/S002199918571039X.
- [41] S. Brinckmann, J.Y. Kim and J.R. Greer, Phys. Rev. Lett. 100 (2008) p. 155502, Available at http://link.aps.org/doi/10.1103/PhysRevLett.100.155502.
- [42] R. Dou and B. Derby, Scripta Mater. 61 (2009) p. 524, Available at http://www. sciencedirect.com/science/article/pii/S1359646209003558.
- [43] A. Stukowski, Modelling Simul. Mater. Sci. Eng. 20 (2012) p. 045021, Available at http://stacks.iop.org/0965-0393/20/i=4/a=045021.
- [44] G. Sainath, P. Rohith and B.K. Choudhary, Philos. Mag. 97 (2017) p. 2632, Available at https://www.tandfonline.com/doi/ref/10.1080/14786435.2017.1347300.
- [45] A. Stukowski, V.V. Bulatov and A. Arsenlis, Modelling Simul. Mater. Sci. Eng. 20 (2012) p. 085007, Available at http://iopscience.iop.org/0965-0393/20/8/ 085007/cites.
- [46] S. Xu and S.Z. Chavoshi, Curr. Appl. Phys. 18 (2018) p. 114, Available at http: //www.sciencedirect.com/science/article/pii/S1567173917302729.